SUPPLEMENTARY MATERIALS

A Bacterial Enzymatic System Neutralizes the Impact of Silica-Magnetite Nanocomposites on ROS Levels

Arina G. Kicheeva[1*] (iD), Ekaterina S. Sushko[1] (iD), Artur A. Dzeranov[2,3,4] (iD), Lyubov S. Bondarenko[2,3] (iD), Natalya S.Tropskaya[2,3] (iD), Kamila A. Kydralieva[2] (iD), Nadezhda S. Kudryasheva[1,5] (iD)

[1]*Institute of Biophysics SB RAS, Federal Research Center 'Krasnoyarsk Science Center SB RAS', Krasnoyarsk, Russia*
[2]*Moscow Aviation Institute (National Research University), Moscow, Russia*
[3]*Sklifosovsky Research Institute for Emergency Medicine, Moscow, Russia*
[4]*Federal Research Center of Problems of Chemical Physics and Medicinal Chemistry, Russian Academy of Sciences, Chernogolovka, Moscow region, Russia*
[5]*School of Fundamental Biology and Biotechnology, Siberian Federal University, Krasnoyarsk, Russia*
(*Corresponding author's e-mail: khyzylsyg@mail.ru)

List of Content

A. Physico-chemical method for nanocomposite characterization

X-ray diffraction. The phase composition and primary particle size of the samples were determined by XRD analysis using the Bragg Brentano geometry on a Philips X'Pert diffractometer (Philips Analytical, Eindhoven, The Netherlands). Cu-Kα radiation (λ = 1.5406 Å) was used as the X-ray source. The collected data were smoothed using the Savitzky–Golay algorithm.[45] Measurements were performed at room temperature, covering an angular range of 30° < 2Θ < 60° with a step size of 0.025° and a dwell time of 1 second per step. Quantitative analysis was performed by refining the entire multiphase spectrum according to the Rietveld method with a fundamental parameter approach [1] using Profex software.

Transmission electron microscopy. The morphology of nanoparticles was studied by scanning and transmission electron microscopy (TEM). The particle morphology was evaluated using a Tecnai G2-20 transmission electron microscope (FEI Company, USA) at an accelerating voltage of 120 kV. All samples were suspended in distilled water using an ultrasound processor (Fisherbrand, USA) at an amplitude of 75% before opalescence. 10 μL of each suspension was applied to carbon-coated copper meshes (200 mesh size) pretreated in a glow discharge cleaning system (PELCO Inc., USA). After incubation for 1 min at room temperature, the excess liquid was carefully removed using filter paper. TEM samples were placed in a TEM holder and further analyzed. The images were obtained using a BM-Ultrascan 1000P CCD camera. The particle size was calculated using the ImageJ program, taking into account at least 100 particles in the image.

Low-temperature nitrogen adsorption. The specific surface area of the samples, the average radius, and the pore size distribution were determined by low-temperature nitrogen adsorption (at 77 K) on an AUTOSORB-1 sorption analyzer (Quantachrome, USA) using the static volumetric method. During the tests, in order to construct nitrogen adsorption isotherms with sorbents, the volume of adsorbate gas (nitrogen) was measured, which was sorbed by the surface of the studied samples when a stationary flow of a gas (He-N_2) mixture of a given composition was passed through them (the volume fraction of N_2 varies from 0 to ≈ 1) at a temperature of liquid nitrogen (77 K) and desorbed when heated (up to about 373 K). Similarly, to construct desorption isotherms, the volume of nitrogen desorbed from the surface of the studied samples was measured with a decrease in its volume fraction in the gas mixture from ≈ 1 to 0. The specific surface area and characteristics of the porous structure of the samples based on the adsorption-desorption isotherms were calculated using the Brunauer-Emmett-Teller (BET) and Barrett–Joyner–Halenda (BJH) methods. Before the start of the tests, the samples were degassed and «thermotrained», which consisted of heating them in a stationary nitrogen stream in a vacuum at a temperature of 423 K in order to remove absorbed gases and vapors from the surface.

B. Physico-chemical characteristics of nanocomposites

Composition, structure and morphology of the samples TA-AA-Fe_3O_4 and TA-HA-Fe_3O_4.

X-ray diffraction (XRD) analysis was used to determine the phase composition of the samples. The presence of amorphous silica complicated the phase identification process by increasing the signal-to-noise ratio in the diffraction patterns. Quantitative Rietveld analysis showed that diffraction patterns of TA-HA-Fe_3O_4 could be interpreted as containing a mixture of iron oxides (magnetite Fe_3O_4, maghemite γ-Fe_2O_3, and ferrihydrite $5Fe_2O_3$ $9H_2O$) and iron oxyhydroxide (goethite α-FeOOH) (Table S1). The corresponding crystal structure files were obtained from the Open Crystallography Database (COD) with the following accession numbers: magnetite: a = 8.4 Å [COD 1011084]; maghemite: a = 8.33 Å [COD 9006316]; ferrihydrite: a = 5.958 Å; c = 8.965 Å [COD 9011573]; goethite: a = 4.5979 Å; b = 9.951 Å; c = 3.0178 Å [COD 2211652] (Figure S1). Rietveld refinement showed that the Fe_3O_4 content in the TA-AA-Fe_3O_4 nanocomposite is close to 100%, reflecting its ideal stoichiometry. AA is known for its ability to act as a one-electron reducing agent, converting Fe(III) to Fe(II) and oxidizing to the ascorbate radical.

TEM images of TA-HA-Fe_3O_4 samples form lamellar structures measuring 33±18 nm in length and 4±2 nm in width, not typical for low-frequency magnetite modified with HA [2–3]. The formation of lamellar structures may be due to the presence of an additional iron oxide phase in addition to magnetite, as indicated by Mossbauer spectroscopic data. The effect of HA on the control of particle size and shape is related both to the blocking of developing faces and to the creation of diffusion restrictions for ionic components [4]. Analysis of the TA-AA-Fe_3O_4 sample showed that the Fe_3O_4 nanoparticles embedded in the TA matrix have an average size of 9±3 nm and have an approximately spherical shape (Figure S2). This size and morphology are characteristic of superparamagnetic particles.

A study of the textural characteristics determining the porosity of the obtained samples (Figure S3) showed that the surface of the particles is a mesoporous structure, a characteristic feature is the presence of hysteresis at the nitrogen adsorption/desorption isotherm. All samples are characterized by type IV isotherms according to the classification, which indicates the course of polymolecular adsorption and the presence of capillary condensation in mesopores. The formation of magnetite NPs in the TA matrix in the presence of HA/AA led to an increase in the specific surface area (SSA) from 90 for TA to 124 and 208 m^2/g for TA-HA-Fe_3O_4 and TA-AA-Fe_3O_4. For the TA-HA-Fe_3O_4 nanocomposite, a significant increase in the specific surface area was observed (Table S2), associated with the formation of an additional phase and a change in the shape of the particles, as indicated by data from XRD and TEM. Several studies [5–8] have also shown that anisotropic non-spherical shapes can have a higher degree of adhesion to target surfaces due to the higher surface area of the interaction.

Using electrophoretic light scattering, zeta potentials were determined over a wide pH range for the original TA matrix and TA-HA-Fe_3O_4 and TA-AA-Fe_3O_4 nanocomposites. Modification with HA/AA and Fe resulted in a shift in the IEP and a decrease in the zeta potential compared to TA (Figure S4).

Results of quantitative analysis of the sample phase composition using the Rietveld method

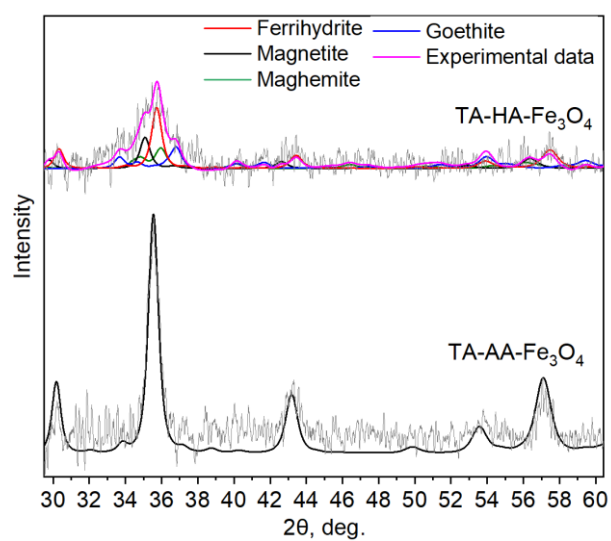| Sample	Phase	γ-Fe_2O_3	Fe_3O_4	$5Fe_2O_3 \cdot 9H_2O$	α-FeOOH	R_{wp}	χ^2
TA-HA-Fe_3O_4	Content in the sample, wt.%	32±4	27±3	15±4	26±5	13.1	0.67
	Lattice parameter, Å	a=8.301	a=8.408	a=5.870 c=9.074	a=4.505 b=9.860 c=2.970		
TA-AA-Fe_3O_4	Content in the sample, wt.%	0	100	0	0	13.9	0.79
	Lattice parameter, Å	-	a=8.388	-	-		

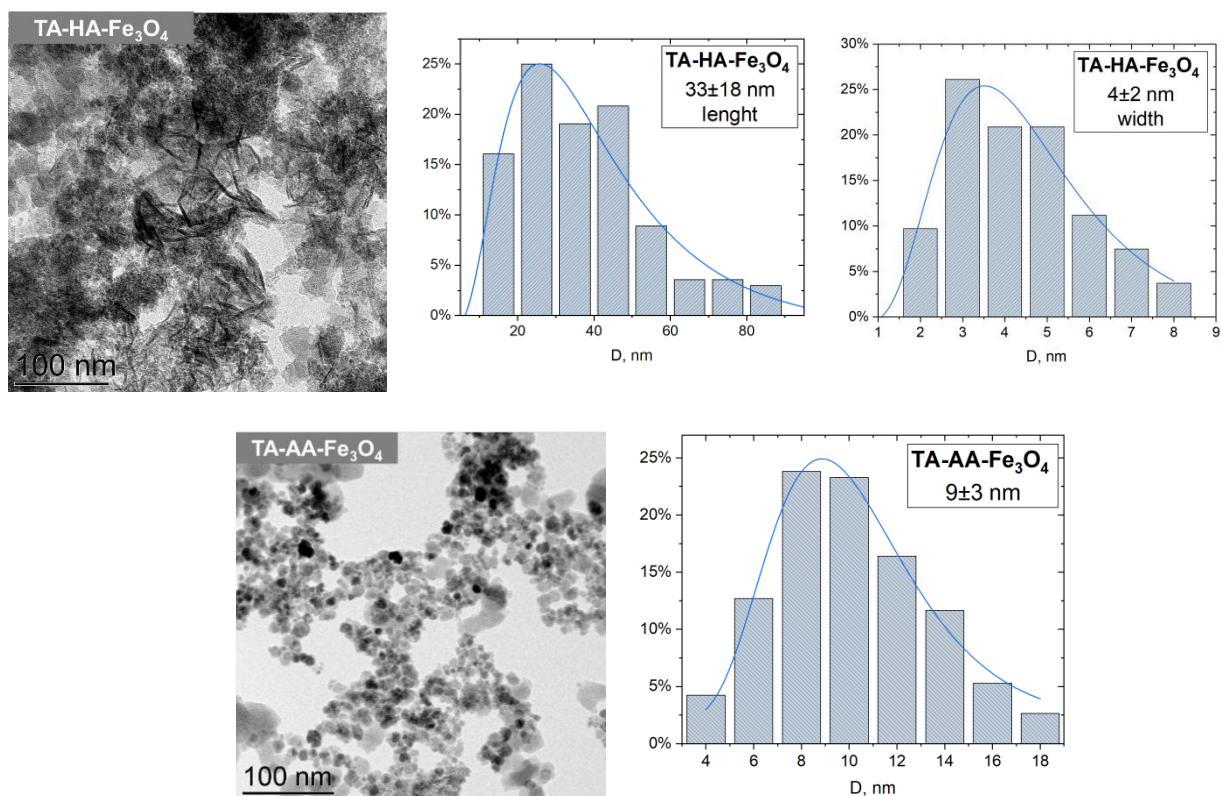Figure S1. XRD patterns of samples TA-HA-Fe_3O_4 and TA-AA-Fe_3O_4

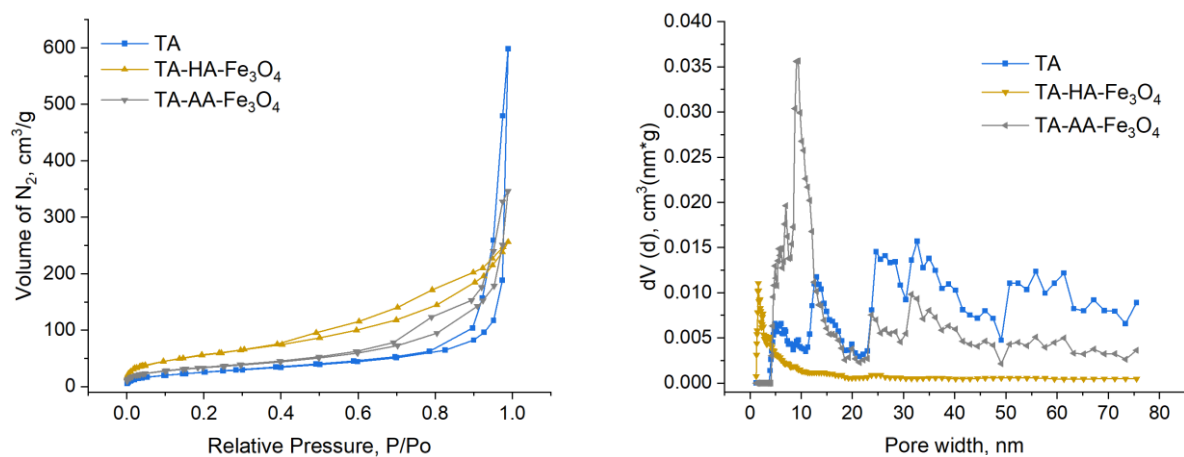Figure S2. TEM micrographs and particle size distribution of samples TA-HA-Fe₃O₄ and TA-AA-Fe₃O₄

Figure S3. Isotherms of low-temperature (77 K) nitrogen adsorption/desorption (a) and pore volume distribution over sample diameters (b)

Textural characteristics of the samples

Sample	SSA_{BET}, (m²/g)	V P/P₀=0.99, (cm³/g)	BJH		NLDFT		t-plot method		
			V, (cm³/g)	d, (nm)	V, (cm³/g)	d, (nm)	V_{micro}, (cm³/g)	SSA_{micro}, (m²/g)	$SSA_{external}$, (m²/g)
TA	90.2	0.85	0.85	23.5	0.6	32.6	-	-	92.2
TA-HA-Fe₃O₄ (1:0.1:1)	208.2	0.40	0.38	3.61	0.37	4.89	-	-	208.2
TA-AA-Fe₃O₄ (1:0.1:1)	124.0	0.54	0.53	8.52	0.46	9.42	-	6.44	117.6

SSA – specific surface area, V – pore volume, d – pore diameter;

BET (Brunauer–Emmett–Teller);

BJH (Barrett–Joyner–Halenda) – a method for determining the volume of mesopores and their size distribution;

NLDFT (Nonlocal Density Functional Theory) (mathematical modeling method) - a method based on the molecular-statistical nonlocal theory of the density of adsorbed fluids;

t-plot – a method for determining the surface area of micropores and estimating the volume of micropores in the presence of mesopores.
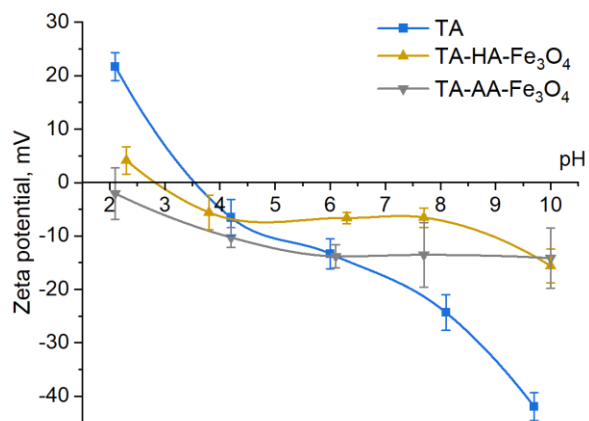
Figure S4. Dependence of the zeta potential of the samples on the pH of the medium
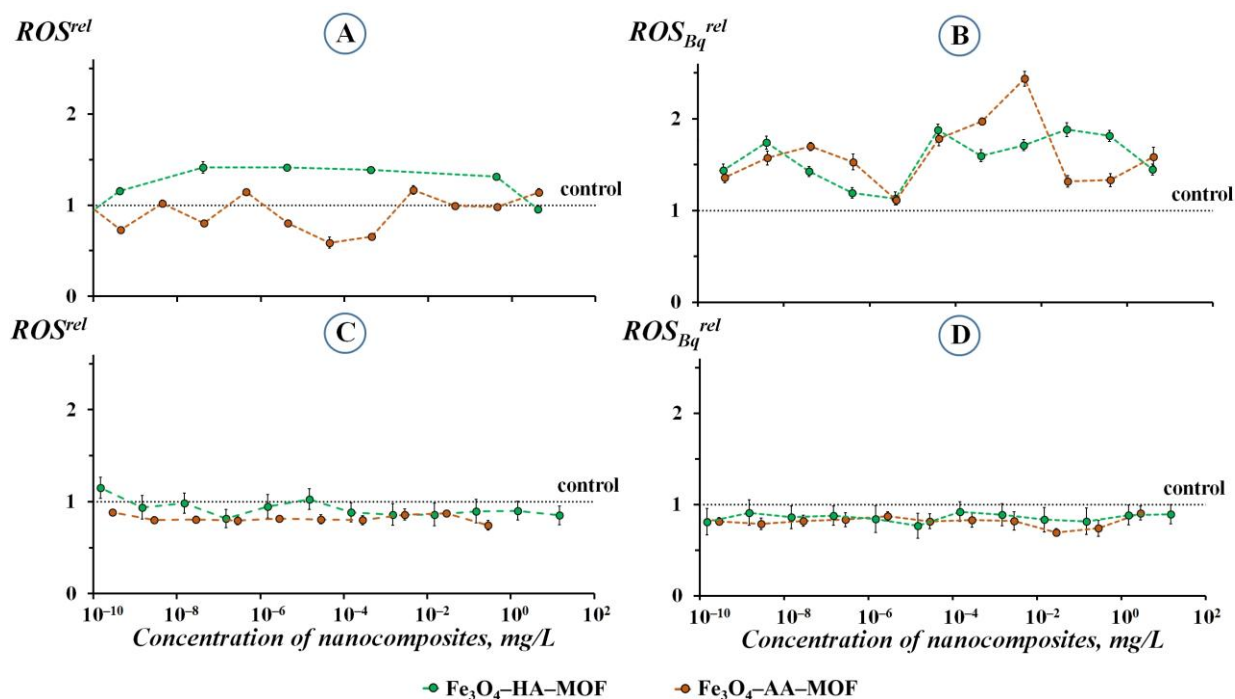
C. Chemiluminescence assay

Figure S5. Relative ROS content: (A) in enzyme-free water solutions, ROS^{rel}; (B) under conditions of oxidative stress in enzyme-free water solutions, $ROS_{Bq}{}^{rel}$; (C) in the enzyme system, ROS^{rel}; (D) under conditions of oxidative stress in the enzyme system, $ROS_{Bq}{}^{rel}$. Control suspension – in the absence of nanocomposites. Conditions of oxidative stress – in the presence of 1,4-benzoquinone ($IC_{50Bq} = 10^{-6}$ M).

D. Bioluminescence assay

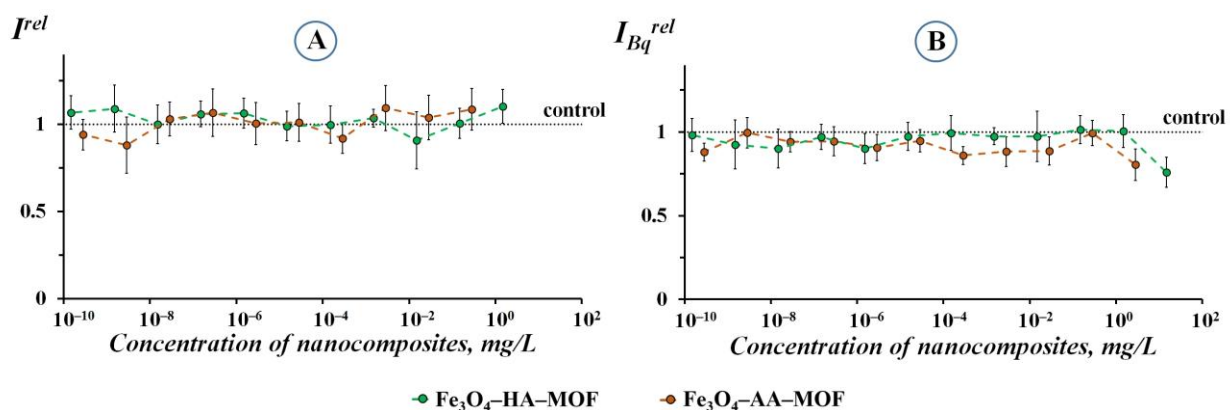$\bullet$ Fe$_3$O$_4$–HA–MOF $\bullet$ Fe$_3$O$_4$–AA–MOF

Figure S6. Relative bioluminescence intensity: (A) in the enzyme system, I^{rel}; (B) under conditions of oxidative stress in the enzyme system, I_{Bq}^{rel}. Control suspension – in the absence of nanocomposites. Conditions of oxidative stress – in the presence of 1,4-benzoquinone ($IC_{50Bq} = 10^{-6}$ M).

References

1 Cheary, R.W. & Coelho, A. (1992). A fundamental parameters approach to X-ray line-profile fitting. *Journal of Applied Crystallography*, *25*(2), 109–121. https://doi.org/10.1107/S0021889891010804.

2 Bayrakci, M., Gezici, O., Bas, S.Z., Ozmen, M., & Maltas, E. (2014). Novel humic acid-bonded magnetite nanoparticles for protein immobilization. *Materials Science and Engineering: C*, *42*,546–552. https://doi.org/10.1016/j.msec.2014.05.066.

3 Rashid, M., Price, N.T., Gracia Pinilla, M.Á., & O'Shea, K.E. (2017). Effective removal of phosphate from aqueous solution using humic acid coated magnetite nanoparticles. *Water Research*, *123*, 353–360. https://doi.org/10.1016/j.watres.2017.06.085.

4 Polyakov, A.Y., Goldt, A.E., Sorkina, T.A., Perminova, I.V., Pankratov, D.A., Goodilin, E.A., & Tretyakov, Y.D. (2012). Constrained growth of anisotropic magnetic δ-FeOOH nanoparticles in the presence of humic substances. *CrystEngComm*, *14*(23), 8097. https://doi.org/10.1039/C2CE25886B.

5 Decuzzi, P., & Ferrari, M. (2006). The adhesive strength of non-spherical particles mediated by specific interactions. *Biomaterials*, *27*(30), 5307–5314. https://doi.org/10.1016/j.biomaterials.2006.05.024.

6 Shah, S., Liu, Y., Hu, W., & Gao, J. (2011). Modeling particle shape-dependent dynamics in nanomedicine. *Journal of Nanoscience and Nanotechnology*, *11*(2), 919–928. https://doi.org/10.1166/jnn.2011.3536.

7 Tao, L., Hu, W., Liu, Y., Huang, G., Sumer, B.D., & Gao, J. (2011). Shape-specific polymeric nanomedicine: emerging opportunities and challenges. *Experimental Biology and Medicine*, *236*(1), 20–29. https://doi.org/10.1258/ebm.2010.010243.

8 Myerson, J.W., Anselmo, A.C., Liu, Y., Mitragotri, S., Eckmann, D.M., & Muzykantov, V.R. (2016). Non-affinity factors modulating vascular targeting of nano- and microcarriers. *Advanced Drug Delivery Reviews*, *99*, 97–112. https://doi.org/10.1016/j.addr.2015.10.011.